Probing the Surface of Oxide Nanoparticles Using DNP-Enhanced High-Resolution NMR of Quadrupolar Nuclei

Hiroki Nagashima, Farahnaz Maleki, Julien Trébosc, Rajesh Belgamwar, Vivek Polshettiwar, Myrtil Kahn, Yoshihiro Kon, Gianfranco Pacchioni, Olivier Lafon, Jean-Paul Amoureux

Probing the Surface of Oxide Nanoparticles Using DNP-Enhanced High-Resolution NMR of Quadrupolar Nuclei

Hiroki Nagashima,[1*] Farahnaz Maleki,[2] Julien Trébosc,[3] Rajesh Belgamwar,[4] Vivek Polshettiwar,[4] Myrtil Kahn,[5] Yoshihiro Kon,[1] Gianfranco Pacchioni,[2] Olivier Lafon,[6*] Jean-Paul Amoureux[6*]

[1] Interdisciplinary Research Center for Catalytic Chemistry, National Institute of Advanced Industrial Science and Technology (AIST), 1-1-1 Higashi, Tsukuba, 305-8565 Ibaraki, Japan.
[2] Dipartimento di Scienza dei Materiali, Università di Milano – Bicocca, via R. Cozzi 55, 20125 Milano, Italy
[3] Univ. Lille, CNRS, Centrale Lille, Univ. Artois, FR 2638, Federation Chevreul, F-59000 Lille, France
[4] Department of Chemical Sciences, Tata Institute of Fundamental Research (TIFR), 400005 Mumbai, India
[5] LCC-CNRS, Université de Toulouse, CNRS, UPS, 31077 Toulouse, France
[6] Univ. Lille, CNRS, Centrale Lille, Univ. Artois, UMR 8181 – UCCS- Unité de Catalyse et de Chimie du Solide, F-59000 Lille, France.

* Corresponding authors: nagashima-hiroki@aist.go.jp olivier.lafon@univ-lille.fr

jean-paul.amoureux@univ-lille.fr

Keywords: oxide nanoparticles; heterogeneous catalysts; solid-state NMR; DNP; half-integer quadrupolar nuclei; MQMAS; CPMG; *D*-RINEPT.

Abstract ≤ 150 words. The surfaces of nanomaterials with applications in optoelectronics and catalysis control their physicochemical properties. NMR spectroscopy, enhanced by dynamic nuclear polarization (DNP), is a powerful approach to probe the local environment of spin-1/2 nuclei near surfaces. However, this technique often lacks robustness and resolution for half-integer quadrupolar nuclei, which represent more than 66% of the NMR-active isotopes. A novel pulse sequence is introduced here to circumvent these issues. This method is applied to observe under high-resolution ^{27}Al and ^{17}O spin-5/2 nuclei on the surface of γ-alumina. Moreover, we report high-resolution ^{17}O spectra of ZnO nanoparticles used in optoelectronics. Their assignment using DFT calculations allows the first NMR observation of O vacancies near the surfaces. Finally, we employ the introduced NMR technique to observe ^{11}B spin-3/2 nuclei on the surface of partially oxidized boron nitride supported on silica and to distinguish its different BO_2OH active sites.

TOC Graphic

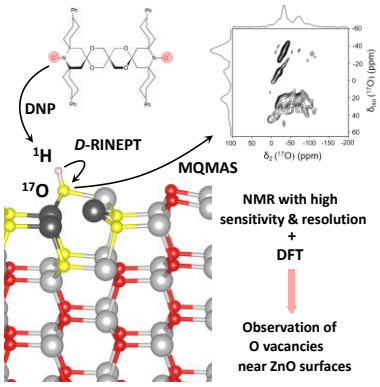

Text ≤ 2500 words. Numerous properties of inorganic nanomaterials depend on the atomic-level assembly of their surfaces. Hence, it is essential to unravel the structure of these regions to improve their applications, notably in heterogeneous catalysis and optoelectronics. Dynamic nuclear polarization (DNP)-enhanced NMR spectroscopy under conditions compatible with the acquisition of high-resolution spectra, *i.e.* at high magnetic field ($B_0 \geq 9.4$ T), under magic-angle spinning (MAS), has been demonstrated as a powerful approach to characterize the surfaces of inorganic materials.[1,2] This approach, named DNP-SENS (surface-enhanced NMR spectroscopy), relies on the transfer of polarization from unpaired electrons to the detected nuclei via a relay through the protons since the ^{1}H-^{1}H spin diffusion efficiently transports the DNP-enhanced ^{1}H polarization in the regions of the samples containing protons.[3] The DNP transfer enhances the NMR sensitivity and facilitates the detection of nuclei near surfaces, which usually represent a small fraction of the total number of nuclei. Furthermore, for inorganic materials, which do not contain hydrogen atoms in their core region, the polarization transfer between protons and the detected isotope, which is only effective up to a few angstroms, allows the selective observation of nuclei located near the surface.[1,2,4]

DNP-SENS of spin-1/2 isotopes, such as ^{13}C, ^{15}N or ^{29}Si, employs under MAS the cross-polarization (CPMAS) technique to transfer the DNP-enhanced ^{1}H polarization to the detected nuclei.[1,2] However, this technique lacks of robustness for half-integer quadrupolar nuclei, which represent 66% of NMR-active isotopes.[5–7] This issue was circumvented by the use of polarization transfers without spin-lock of the quadrupolar nuclei, such as PRESTO (phase-shifted recoupling effects a smooth transfer of order),[8] and more recently *D*-RINEPT (dipolar-mediated refocused INEPT).[9,10] This last transfer is usually more robust and efficient than CPMAS and PRESTO, especially for quadrupolar nuclei subject to small dipolar couplings with protons, such as those distant from protons or with low gyromagnetic ratio (γ).

Another challenge for the DNP-SENS of quadrupolar nuclei is the lack of resolution since the central transition between the ±1/2 energy levels is broadened by the second-order quadrupolar interaction.[11] This broadening has been refocused using an MQMAS (multiple-quantum MAS) filter.[12,13] However, these experiments were not optimal since they relied either on the use of CPMAS transfers between protons and quadrupolar nuclei,[12] which decrease their robustness, or on direct DNP transfers between unpaired electrons and these quadrupolar isotopes,[13] which are usually less selective and sensitive than indirect DNP with ^{1}H relay for the observation of surfaces.

We introduce herein a novel high-resolution DNP-SENS experiment for quadrupolar nuclei, which combines *D*-RINEPT and MQMAS techniques. This novel method is demonstrated to observe ^{17}O, ^{27}Al and ^{11}B nuclei near surfaces and it allows gaining new insights into the atomic-level structure of oxide nanoparticles used for optoelectronics and heterogeneous catalysis, including γ-alumina,[13–15] ZnO nanocrystals,[16–18] and partially oxidized boron nitride supported on dendritic and fibrous nanosilica (BN-B_2O_3/DFNS).[19]

The new *D*-RINEPT-MQMAS pulse sequence is shown in Fig.**S1**. The DNP-enhanced ^{1}H polarization is first transferred to the half-integer quadrupolar isotope, *S*, using *D*-RINEPT with composite-pulses, continuous-wave irradiation between the recoupling blocks, and heteronuclear dipolar recoupling based on the $SR4_1^2$ symmetry and built from tanh/tan adiabatic inversion pulses.[9,10] Then, the anisotropic part of the second-order quadrupolar dephasing is refocused using a split-t_1 amplitude-modulated MQMAS filter, for which triple- and single-quantum (denoted 3Q and 1Q, respectively) coherences evolve during t_1 and Rt_1 delays, respectively, with R = 7/9 and 19/12 for S = 3/2 and 5/2, respectively.[20,21] In this MQMAS variant using a z-filter, both echo and antiecho coherence pathways contribute to the processed signal with equal amplitude to obtain pure absorption lineshapes. Moreover, as these two pathways are refocused simultaneously, the sensitivity can be improved easily through a train of quadrupolar Carr-Purcell Meiboom-Gill (CPMG) echoes.[22,23] It has been shown that for

radical concentrations typically employed in MAS DNP experiments, significant sensitivity enhancements can still be obtained by CPMG detection, even if the unpaired electrons reduce the transverse dephasing time, T_2', in a Hahn echo experiment.[24] The conversion between 1Q and 3Q coherences of the *S* spin is improved using FAM-*N* (fast amplitude modulated *N* pulses).[25,26] The desired coherence transfer pathways for this sequence were selected using phase cycles consisting of 88 and 64 steps for $S = 3/2$ and 5/2, respectively. All spectra were recorded at 105 K with $B_0 = 9.4$ T and $\nu_R = 12.5$ kHz (except in Fig.**S6**) and all samples were impregnated with a TEKPol solution in TCE (1,1,2,2-tetrachloroethane) (see Section S2).

The proposed *D*-RINEPT-MQMAS experiment was initially tested to observe the ^{27}Al nuclei, with 100% natural abundance (*NA*), near the surface of γ-alumina. Fig.**1a** shows the DNP-enhanced 2D ^{1}H → ^{27}Al *D*-RINEPT-MQMAS spectrum recorded with $\tau_{dip} = 0.4$ ms. This spectrum is dominated by the AlO_4 and AlO_6 signals with peak positions of $(\delta_{iso}^{CS,QIS}, \delta_2) \approx (84, 66)$ and (16, 8) ppm, respectively. Nevertheless, a small signal at $(\delta_{iso}^{CS,QIS}, \delta_2) \approx (46, 34)$ ppm is also detected and is assigned to AlO_5 sites, which reside mainly on the surface of γ-alumina.[14,27,28] This signal, which is masked by that of AlO_4 in 1D ^{1}H → ^{27}Al *D*-RINEPT spectra,[10] is more easily detected in Fig.**1a** than in the previously reported DNP-enhanced 2D ^{1}H → ^{27}Al CP-MQMAS spectrum of γ-alumina impregnated with bTbk solution and acquired within 7 h,[14] owing to the sensitivity improvements yielded by the use of TEKPol polarizing agent, quadrupolar CPMG (QCPMG) detection and *D*-RINEPT transfer. For longer recoupling time, $\tau_{dip} = 1.2$ ms, the DNP-enhanced ^{1}H polarization is transferred to ^{27}Al nuclei below the surface since the *D*-RINEPT transfer is not affected by dipolar truncation, contrary to the CPMAS scheme,[9,10,14] and the AlO_5 surface signal is no longer visible in the 2D spectrum shown in Fig.**1b** since it decays under ^{1}H-^{27}Al dipolar interactions.[9] Moreover, the relative intensity of the AlO_6 signal decreases for longer recoupling, which suggests a larger amount of AlO_6 sites near the surface of hydrated γ-alumina nanoparticles in agreement with structural models and previous NMR observations.[14,27]

The *D*-RINEPT-MQMAS experiment was then applied to observe the local environment of ^{17}O nuclei near the surface of γ-alumina nanoparticles. For this sample, it has been shown that sensitivity gain provided by DNP allows the acquisition of 1D ^{1}H → ^{17}O *D*-RINEPT-QCPMG spectra in few hours in natural abundance (*NA* = 0.038% for ^{17}O).[9] Therefore, 2D experiments involving ^{17}O isotope are unpractical without isotopic enrichment. To enhance the sensitivity, the γ-alumina nanoparticles were enriched in ^{17}O isotope using grinding assisted by ^{17}O-labeled water (section **S2**).[29] Almost a three-fold larger DNP enhancement was achieved when grinding was carried out using zirconia jar and balls, instead of stainless steel (Fig.**S2**). The lower DNP enhancement in the case of stainless steel may stem from the incorporation of ferro- or para-magnetic impurities in the γ-alumina sample, which accelerate the longitudinal nuclear relaxations and hence, reduce the DNP transfer efficiency. The DNP-enhanced 2D ^{1}H → ^{27}Al *D*-RINEPT-MQMAS spectrum of γ-alumina using $\tau_{dip} = 0.4$ ms is not significantly modified after the liquid-assisted grinding, as seen in Fig.**S3**. Hence, this procedure does not alter the atomic-level structure of the γ-alumina surface. Moreover, the ^{1}H → ^{17}O *D*-RINEPT 1D spectra shown in Fig.**S4** are also similar to those recently reported for isotopically unmodified γ-alumina.[9]

The ^{1}H→^{17}O *D*-RINEPT-MQMAS 2D spectra of γ-alumina nanoparticles recorded with short or long dipolar recoupling times are shown in Fig.**2** and their simulations with the NMR parameters given in Table **S2** are displayed in Fig.**S5**. For $\tau_{dip} = 40$ μs, the 2D spectrum (Fig.**2a**), only exhibits a single resonance assigned to Al_yOH sites (y = 1 or 2), which are subject to large quadrupolar interactions with $C_Q \approx 6.1$ MHz (Table **S2**), owing to their covalent bond with hydrogen atom. This signal decays rapidly under ^{1}H-^{17}O dipolar couplings and for $\tau_{dip} = 1.12$ ms, the 1D *D*-RINEPT spectrum is dominated by overlapping signals of unprotonated OAl_x

sites with x = 3 or 4 (Fig.**S4**).[13,15] Conversely, the 2D spectrum acquired with similar recoupling time (1.04 ms) shown in Fig.**2b** allows resolving the signals of two OAl_4 sites subject to low quadrupolar interaction ($C_Q \approx$ 1.2-1.3 MHz) and one OAl_3 environment with a larger $C_Q \approx$ 2.6 MHz, owing to lower symmetry. The shielded and deshielded OAl_4 signals, with isotropic chemical shifts, δ_{iso}^{CS} = 61 and 72 ppm, were assigned to subsurface and surface sites, respectively.[15] The 2D spectra were acquired in about 2 h, a time comparable to that of 2D ^{17}O MQMAS experiments enhanced by direct DNP on γ-alumina enriched using $^{17}O_2$ gas.[13]

We then applied the *D*-RINEPT-MQMAS experiment to probe the O sites near the surface of ZnO nanoparticles stabilized or not by dodecylamine (DDA) ligands (denoted ZnO@DDA). As 2D experiments involving ^{17}O nuclei cannot be acquired in natural abundance, these samples were labelled using ^{17}O-enriched water during the synthesis for ZnO@DDA or liquid-assisted grinding for ZnO. As seen in Fig.**S6**, the DNP-enhanced $^1H \rightarrow ^{17}O$ *D*-RINEPT 1D spectra of these nanoparticles acquired with short recoupling times exhibit a broad signal, which decreases for longer τ_{dip} delay and hence, must stem from O atoms close to protons. This broad signal overlaps for $\tau_{dip} \approx$ 500 μs with a narrower signal near −30 ppm, which is more shielded and broader than the peak at −18 ppm visible in the direct excitation spectrum and assigned to core O atoms.[17,30,31] Furthermore, a broad resonance with a maximum around 50 ppm is also detected (Fig.**S7**).

The $^1H \rightarrow ^{17}O$ *D*-RINEPT-MQMAS 2D spectra of ZnO@DDA recorded with three different τ_{dip} delays are shown in Fig.**3** and their simulations with the NMR parameters given in Table **S3** are displayed in Fig.**S8**. Similar spectra were recorded for ZnO (Fig.**S9**). No signal resonating near $\delta_2 \approx$ 50 ppm was detected in the 2D *D*-RINEPT-MQMAS spectra because of the low intensity of this signal.

DFT calculations of NMR parameters on ZnO slabs were carried out to help the assignment of ^{17}O signals (Fig.**S10** and Table **S4**). The signal with $\delta_{iso}^{CS} = -33$ ppm and $C_Q <$ 0.5 MHz, which is detected for the longest recoupling time (Fig.**3c** and Table **S3**), exhibits NMR parameters close to OZn_4 sites located in, or below, the second subsurface atomic layer (sites 4-7 in Table **S4**). The minimal distance between the proton on the surface and these OZn_4 sites is at least of 7 Å, and hence these sites are mostly observed for long recoupling times. However, a ZnO slab devoid of vacancies and hydrogen atoms cannot account for the other signals with large δ_{iso}^{CS} and C_Q values. Therefore, we carried DFT calculations of NMR parameters for different ZnO structural models containing protons and O vacancies in different locations. The slabs we have used are shown in Figs.**S11** to **S16** and the corresponding DFT parameters are given in Tables **S5** to **S10**. Based on these calculations, the nuclei with $\delta_{iso}^{CS} = -4.5$ ppm and C_Q = 5.6 MHz (Table **S3**), which are the closest to protons, must correspond to $HOZn_3$ sites near surface vacancy (e.g. site 2 in Table **S9**), whereas those with $\delta_{iso}^{CS} = -6.1$ ppm and C_Q = 4.8 MHz (Table **S3**), which are slightly more distant from protons, must stem from unprotonated surface OZn_3 sites near surface O vacancy (which according to DFT calculations, are subject to large quadrupolar interactions, as seen in Tables **S7** and **S8**).

Furthermore, the subsurface ^{17}O nuclei near O vacancy exhibit isotropic chemical shifts ranging from 15 to 81 ppm (sites 7 to 11 in Table **S6**), which could account for the broad signal with a maximum near 50 ppm detected in the 1D $^1H \rightarrow ^{17}O$ *D*-RINEPT spectra (Fig.**S7**). The other signals detected for τ_{dip} = 640 μs with $-38.2 \text{ ppm} \leq \delta_{iso}^{CS} \leq -3.3$ ppm and $C_Q \leq$ 1.8 MHz could stem from OZn_4 sites located in the first atomic layer below the surface. The presence of O vacancies near the surface increases their C_Q values (compare Tables **S4** and **S9**). Hence, the combination of these NMR data and DFT calculations proves the presence of O vacancy in the subsurface and on the surface of ZnO@DDA and ZnO. To the best of our knowledge, these results represent the first direct NMR observation of O vacancies near oxide surfaces.[32] This is an important achievement since these point defects strongly influence the optoelectronic and

catalytic properties of oxide surfaces, but their atomic-level structure is challenging to characterize owing to their low amount and their lack of long-range order.

D-RINEPT-MQMAS experiments were demonstrated in the case of spin-3/2 isotope by observing ^{11}B nuclei (*NA* = 80.1%) near the surface of BN-B_2O_3/DFNS, which has been recently demonstrated as an efficient catalyst for the oxidative dehydrogenation of propane.[19] Direct excitation spectra shown in Figs.**S17a** and **S17b** exhibit overlapping signals of BN_3, BO_3 and BO_4 sites. Direct DNP enhances more the BN_3 signal with respect to those of BO_3 and BO_4 environments. This result is consistent with the slower longitudinal relaxation of $^{11}BN_3$ nuclei ($T_1 \approx 7.3$ s for BN_3 instead of 5.1 s for BO_3/BO_4,), which improves the efficiency of electron $\rightarrow$ ^{11}B transfer and spin diffusion.[33] Conversely, as seen in Figs.**S17c** and **S17d**, the DNP-enhanced 1D ^{1}H $\rightarrow$ ^{11}B *D*-RINEPT spectra only show the signal of BO_3 and BO_4 groups, indicating that the surface and subsurface of BN-B_2O_3/DFNS mainly consist of boron oxide. The $^{11}BN_3$ site is observed by direct DNP but not by indirect DNP due to the longer range of hyperfine couplings compared to ^{1}H-^{11}B dipolar interactions.[4] This result proves that the BN_3 phase is located more than a few angstroms below the surface and is oxidized into boron oxide.[19]

Nevertheless, the 1D ^{11}B spectra alone do not allow to resolve the different boron environments. To circumvent this issue, we recorded the 2D ^{11}B MQMAS spectra of BN-B_2O_3/DFNS. The ^{11}B MQMAS spectrum shown in Fig.**4a** acquired using the z-filter sequence,[34] and enhanced by direct DNP allows resolving four ^{11}B signals assigned to BN_3, BN_2O, BO_3 and BO_4 groups.[19] Moreover, the ^{1}H$\rightarrow$^{11}B *D*-RINEPT-MQMAS 2D spectra acquired using the pulse sequence shown in Fig.**S1b** provide additional information on the proximity with protons. The spectrum with τ_{dip} = 0.32 ms, shown in Fig.**4b**, allows the selective observation of ^{11}B nuclei covalently bonded to OH groups and exhibits four ^{11}B signals assigned by decreasing isotropic shift to BO_2OH groups residing in boroxol ring or chain, $B(OSi)_x(OB)_{3-x}OH$ with $0 \leq x \leq 3$ and $B(OB)_3OH$ (Fig.**S18c**).[19] In particular, this spectrum allows to resolve clearly the signals of the two types of BO_2OH groups, which have been identified as the active sites for the catalytic oxidative dehydrogenation of propane.[19,35,36] In the MQMAS spectrum of Fig.**4a**, their signals are overlapped by those of unprotonated BO_3 species. For longer τ_{dip} delays, these signals decrease and the MQMAS spectrum is dominated by those of unprotonated BO_3 and BO_4 sites (Figs.**4c** and **S18b**).

In conclusion, we demonstrated the possibility to acquire high-resolution spectra of spin-3/2 and 5/2 isotopes near the surface of inorganic nanoparticles by combining DNP, *D*-RINEPT, MQMAS and QCPMG techniques. This novel DNP-SENS experiment was applied to observe surface and subsurface ^{27}Al and ^{17}O nuclei in γ-alumina. Furthermore, the assignment of high-resolution ^{17}O DNP-SENS spectra of ZnO nanoparticles with the help of DFT demonstrates for the first time the possibility to observe O vacancies near oxide surfaces using NMR. Finally, this experiment was applied to distinguish the different BO_2OH groups, which form the active sites on the surface of BN-B_2O_3/DFNS for the catalytic oxidative dehydrogenation of propane.

Supporting Information: Pulse sequences of *D*-RINEPT-MQMAS-QCPMG; Experimental details; DNP-enhanced NMR spectra of γ-alumina, Zn^{17}O and BN-B_2O_3/DFNS; Structural models of ZnO slabs and corresponding NMR parameters calculated by DFT.

Acknowledgements: Chevreul Institute (FR 2638), Ministère de l'Enseignement Supérieur et de la Recherche, Hauts-de-France Region, and FEDER are acknowledged for supporting and funding partially this work. The authors wish to thank Dr Yannick Coppel for helpful discussion regarding the assignment of ^{17}O NMR signals of ZnO nanoparticles. Financial support from the IR INFRANALYTICS FR2054 CNRS for conducting the research is gratefully acknowledged. H.N. acknowledges JSPS Grant-in-Aid for Early-Career Scientists (JP20K15319) and JST, PRESTO Grant Number JPMJPR2276, Japan

References:

(1) Lesage, A.; Lelli, M.; Gajan, D.; Caporini, M. A.; Vitzthum, V.; Miéville, P.; Alauzun, J.; Roussey, A.; Thieuleux, C.; Mehdi, A.; Bodenhausen, G.; Copéret, C.; Emsley, L. Surface Enhanced NMR Spectroscopy by Dynamic Nuclear Polarization. *J. Am. Chem. Soc.* **2010**, *132* (44), 15459–15461.

(2) Berruyer, P.; Emsley, L.; Lesage, A. DNP in Materials Science: Touching the Surface. *eMagRes* **2018**, *7*, 93–104.

(3) Lafon, O.; Thankamony, A. S. L.; Kobayashi, T.; Carnevale, D.; Vitzthum, V.; Slowing, I. I.; Kandel, K.; Vezin, H.; Amoureux, J.-P.; Bodenhausen, G.; Pruski, M. Mesoporous Silica Nanoparticles Loaded with Surfactant: Low Temperature Magic Angle Spinning ^{13}C and ^{29}Si NMR Enhanced by Dynamic Nuclear Polarization. *J. Phys. Chem. C* **2013**, *117* (3), 1375–1382.

(4) Lafon, O.; Rosay, M.; Aussenac, F.; Lu, X.; Trébosc, J.; Cristini, O.; Kinowski, C.; Touati, N.; Vezin, H.; Amoureux, J.-P. Beyond the Silica Surface by Direct Silicon-29 Dynamic Nuclear Polarization. *Angew. Chem., Int. Ed.* **2011**, *50* (36), 8367–8370.

(5) Vega, A. J. CP/MAS of Quadrupolar S = 3/2 Nuclei. *Solid State Nucl. Magn. Reson.* **1992**, *1* (1), 17–32.

(6) Amoureux, J.-P.; Pruski, M. Theoretical and Experimental Assessment of Single-and Multiple-Quantum Cross-Polarization in Solid State NMR. *Mol. Phys.* **2002**, *100*, 1595–1613.

(7) Ashbrook, S. E.; Wimperis, S. Spin-Locking of Half-Integer Quadrupolar Nuclei in Nuclear Magnetic Resonance of Solids: Second-Order Quadrupolar and Resonance Offset Effects. *J. Chem. Phys.* **2009**, *131* (19), 194509.

(8) Perras, F. A.; Kobayashi, T.; Pruski, M. Natural Abundance ^{17}O DNP Two-Dimensional and Surface-Enhanced NMR Spectroscopy. *J. Am. Chem. Soc.* **2015**, *137* (26), 8336–8339.

(9) Nagashima, H.; Trébosc, J.; Kon, Y.; Sato, K.; Lafon, O.; Amoureux, J.-P. Observation of Low-γ Quadrupolar Nuclei by Surface-Enhanced NMR Spectroscopy. *J. Am. Chem. Soc.* **2020**, *142* (24), 10659–10672.

(10) Nagashima, H.; Trébosc, J.; Kon, Y.; Lafon, O.; Amoureux, J.-P. Efficient Transfer of DNP-Enhanced ^{1}H Magnetization to Half-Integer Quadrupolar Nuclei in Solids at Moderate Spinning Rate. *Magn. Reson. Chem.* **2021**, *59* (9–10), 920–939.

(11) Ashbrook, S. E.; Sneddon, S. New Methods and Applications in Solid-State NMR Spectroscopy of Quadrupolar Nuclei. *J. Am. Chem. Soc.* **2014**, *136* (44), 15440–15456.

(12) Vitzthum, V.; Mieville, P.; Carnevale, D.; Caporini, M. A.; Gajan, D.; Copéret, C.; Lelli, M.; Zagdoun, A.; Rossini, A. J.; Lesage, A.; Emsley, L.; Bodenhausen, G. Dynamic Nuclear Polarization of Quadrupolar Nuclei Using Cross Polarization from Protons: Surface-Enhanced Aluminium-27 NMR. *Chem. Commun.* **2012**, *48* (14), 1988–1990.

(13) Li, W.; Wang, Q.; Xu, J.; Aussenac, F.; Qi, G.; Zhao, X.; Gao, P.; Wang, C.; Deng, F. Probing the Surface of γ-Al_2O_3 by Oxygen-17 Dynamic Nuclear Polarization Enhanced Solid-State NMR Spectroscopy. *Phys. Chem. Chem. Phys.* **2018**, *20* (25), 17218–17225.

(14) Lee, D.; Duong, N. T.; Lafon, O.; De Paëpe, G. Primostrato Solid-State NMR Enhanced by Dynamic Nuclear Polarization: Pentacoordinated Al^{3+} Ions Are Only Located at the Surface of Hydrated γ-Alumina. *J. Phys. Chem. C* **2014**, *118*, 25065−25076.

(15) Wang, Q.; Li, W.; Hung, I.; Mentink-Vigier, F.; Wang, X.; Qi, G.; Wang, X.; Gan, Z.; Xu, J.; Deng, F. Mapping the Oxygen Structure of γ-Al_2O_3 by High-Field Solid-State NMR Spectroscopy. *Nat. Commun.* **2020**, *11* (1), 3620.

(16) Champouret, Y.; Coppel, Y.; Kahn, M. L. Evidence for Core Oxygen Dynamics and Exchange in Metal Oxide Nanocrystals from In Situ ^{17}O MAS NMR. *J. Am. Chem. Soc.* **2016**, *138* (50), 16322–16328.

(17) Spataro, G.; Champouret, Y.; Florian, P.; Coppel, Y.; Kahn, M. L. Multinuclear Solid-State NMR Study: A Powerful Tool for Understanding the Structure of ZnO Hybrid Nanoparticles. *Phys. Chem. Chem. Phys.* **2018**, *20* (18), 12413–12421.
(18) Wang, Y.; Coppel, Y.; Lepetit, C.; Marty, J.-D.; Mingotaud, C.; Kahn, M. L. Anisotropic Growth of ZnO Nanoparticles Driven by the Structure of Amine Surfactants: The Role of Surface Dynamics in Nanocrystal Growth. *Nanoscale Adv.* **2021**, *3* (21), 6088–6099.
(19) Belgamwar, R.; Rankin, A. G. M.; Maity, A.; Mishra, A. K.; Gómez, J. S.; Trébosc, J.; Vinod, C. P.; Lafon, O.; Polshettiwar, V. Boron Nitride and Oxide Supported on Dendritic Fibrous Nanosilica for Catalytic Oxidative Dehydrogenation of Propane. *ACS Sustain. Chem. Eng.* **2020**, *8* (43), 16124–16135.
(20) Brown, S. P.; Heyes, S. J.; Wimperis, S. Two-Dimensional MAS Multiple-Quantum NMR of Quadrupolar Nuclei. Removal of Inhomogeneous Second-Order Broadening. *J. Magn. Reson. A* **1996**, *119* (2), 280–284.
(21) Brown, S. P.; Wimperis, S. Two-Dimensional Multiple-Quantum MAS NMR of Quadrupolar Nuclei: A Comparison of Methods. *J. Magn. Reson.* **1997**, *128* (1), 42–61.
(22) Vosegaard, T.; Larsen, F. H.; Jakobsen, H. J.; Ellis, P. D.; Nielsen, N. C. Sensitivity-Enhanced Multiple-Quantum MAS NMR of Half-Integer Quadrupolar Nuclei. *J. Am. Chem. Soc.* **1997**, *119* (38), 9055–9056.
(23) Lefort, R.; Wiench, J. W.; Pruski, M.; Amoureux, J.-P. Optimization of Data Acquisition and Processing in Carr–Purcell–Meiboom–Gill Multiple Quantum Magic Angle Spinning Nuclear Magnetic Resonance. *J. Chem. Phys.* **2002**, *116* (6), 2493–2501.
(24) Rossini, A. J.; Zagdoun, A.; Lelli, M.; Gajan, D.; Rascón, F.; Rosay, M.; Maas, W. E.; Copéret, C.; Lesage, A.; Emsley, L. One Hundred Fold Overall Sensitivity Enhancements for Silicon-29 NMR Spectroscopy of Surfaces by Dynamic Nuclear Polarization with CPMG Acquisition. *Chem. Sci.* **2011**, *3* (1), 108–115.
(25) Colaux, H.; Dawson, D. M.; Ashbrook, S. E. Efficient Amplitude-Modulated Pulses for Triple- to Single-Quantum Coherence Conversion in MQMAS NMR. *J. Phys. Chem. A* **2014**, *118* (31), 6018–6025.
(26) Colaux, H.; Dawson, D. M.; Ashbrook, S. E. Investigating FAM-N Pulses for Signal Enhancement in MQMAS NMR of Quadrupolar Nuclei. *Solid State Nucl. Magn. Reson.* **2017**, *84*, 89–102.
(27) Digne, M. Use of DFT to Achieve a Rational Understanding of Acid-Basic Properties of γ-Alumina Surfaces. *J. Catal.* **2004**, *226* (1), 54–68.
(28) Kwak, J.; Hu, J.; Kim, D.; Szanyi, J.; Peden, C. Penta-Coordinated Al^{3+} Ions as Preferential Nucleation Sites for BaO on γ-Al_2O_3: An Ultra-High-Magnetic Field ^{27}Al MAS NMR Study. *J. Catal.* **2007**, *251* (1), 189–194.
(29) Chen, C.-H.; Gaillard, E.; Mentink-Vigier, F.; Chen, K.; Gan, Z.; Gaveau, P.; Rebière, B.; Berthelot, R.; Florian, P.; Bonhomme, C.; Smith, M. E.; Métro, T.-X.; Alonso, B.; Laurencin, D. Direct ^{17}O Isotopic Labeling of Oxides Using Mechanochemistry. *Inorg. Chem.* **2020**, *59* (18), 13050–13066.
(30) Turner, G. L.; Chung, S. E.; Oldfield, E. Solid-State Oxygen-17 Nuclear Magnetic Resonance Spectroscopic Study of the Group 11 Oxides. *J. Magn. Reson. 1969* **1985**, *64* (2), 316–324.
(31) Song, B.; Li, Y.; Wu, X.-P.; Wang, F.; Lin, M.; Sun, Y.; Jia, A.; Ning, X.; Jin, L.; Ke, X.; Yu, Z.; Yang, G.; Hou, W.; Ding, W.; Gong, X.-Q.; Peng, L. Unveiling the Surface Structure of ZnO Nanorods and H_2 Activation Mechanisms with ^{17}O NMR Spectroscopy. *J. Am. Chem. Soc.* **2022**, *144* (51), 23340–23351.
(32) Pacchioni, G.; Rahman, T. S. Defect Engineering of Oxide Surfaces: Dream or Reality? *J. Phys. Condens. Matter* **2022**, *34* (29), 291501.

(33) Björgvinsdóttir, S.; Walder, B. J.; Pinon, A. C.; Emsley, L. Bulk Nuclear Hyperpolarization of Inorganic Solids by Relay from the Surface. *J. Am. Chem. Soc.* **2018**, *140* (25), 7946–7951.
(34) Amoureux, J.-P.; Fernandez, C.; Steuernagel, S. Z-Filtering in MQMAS NMR. *J. Magn. Reson. A* **1996**, *123* (1), 116–118.
(35) Love, A. M.; Thomas, B.; Specht, S. E.; Hanrahan, M. P.; Venegas, J. M.; Burt, S. P.; Grant, J. T.; Cendejas, M. C.; McDermott, W. P.; Rossini, A. J.; Hermans, I. Probing the Transformation of Boron Nitride Catalysts under Oxidative Dehydrogenation Conditions. *J. Am. Chem. Soc.* **2019**, *141* (1), 182–190.
(36) Love, A. M.; Cendejas, M. C.; Thomas, B.; McDermott, W. P.; Uchupalanun, P.; Kruszynski, C.; Burt, S. P.; Agbi, T.; Rossini, A. J.; Hermans, I. Synthesis and Characterization of Silica-Supported Boron Oxide Catalysts for the Oxidative Dehydrogenation of Propane. *J. Phys. Chem. C* **2019**, *123* (44), 27000–27011.

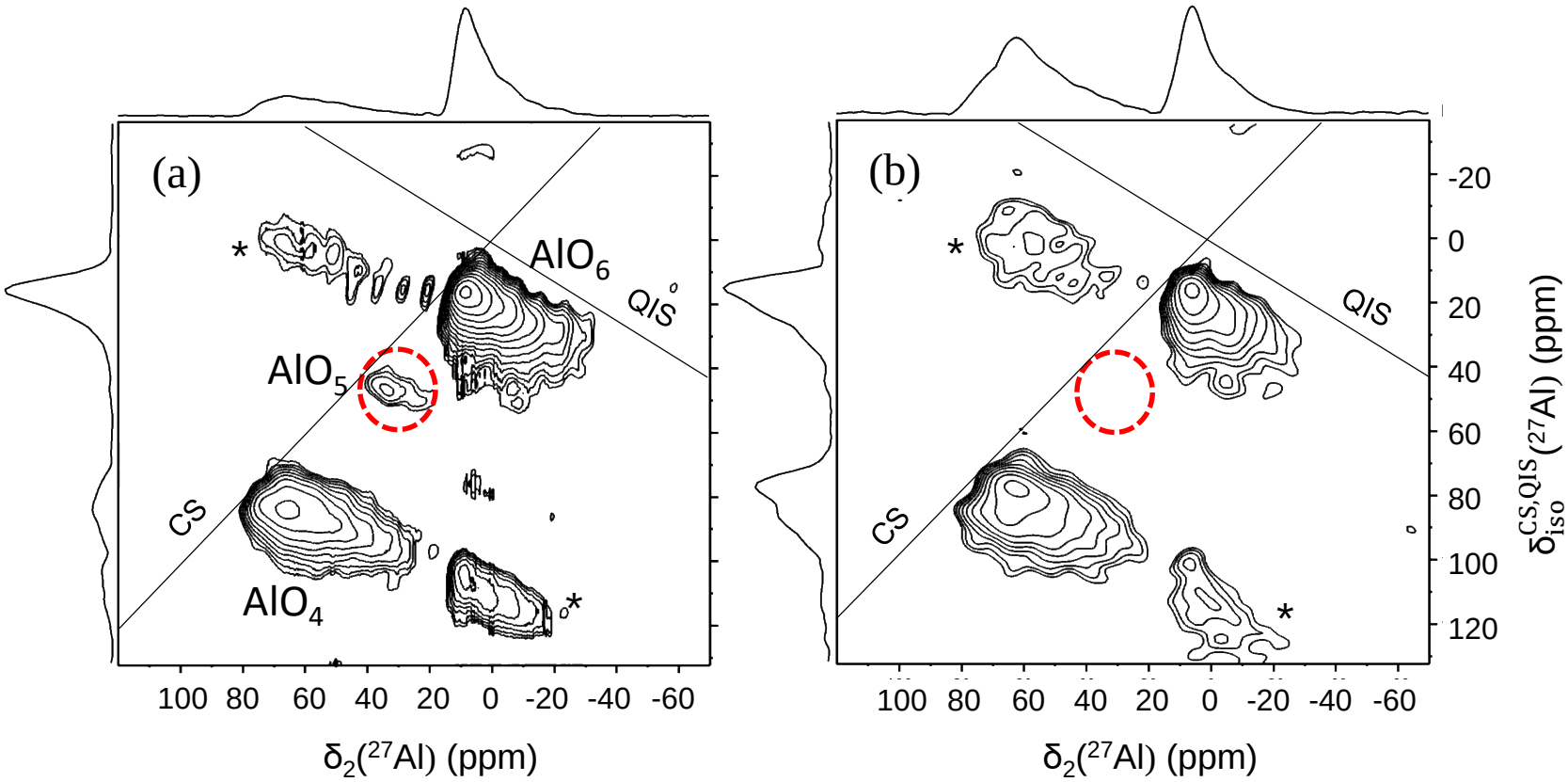

Fig.1. DNP-enhanced 2D $^{1}H \rightarrow {}^{27}Al$ *D*-RINEPT-MQMAS-QCPMG spectra along with their skyline projections in both dimensions of γ-alumina impregnated with 8 mM TEKPol solution acquired with τ_{dip} = (a) 0.4 and (b) 1.2 ms, and 8 QCPMG echoes. The symbol * denotes spinning sidebands. The isotropic chemical shift (CS) axis and quadrupolar-induced shift (QIS) direction are displayed since the isotropic chemical shift of a resonance can be determined by projection of its center of gravity on the CS axis along the QIS direction.

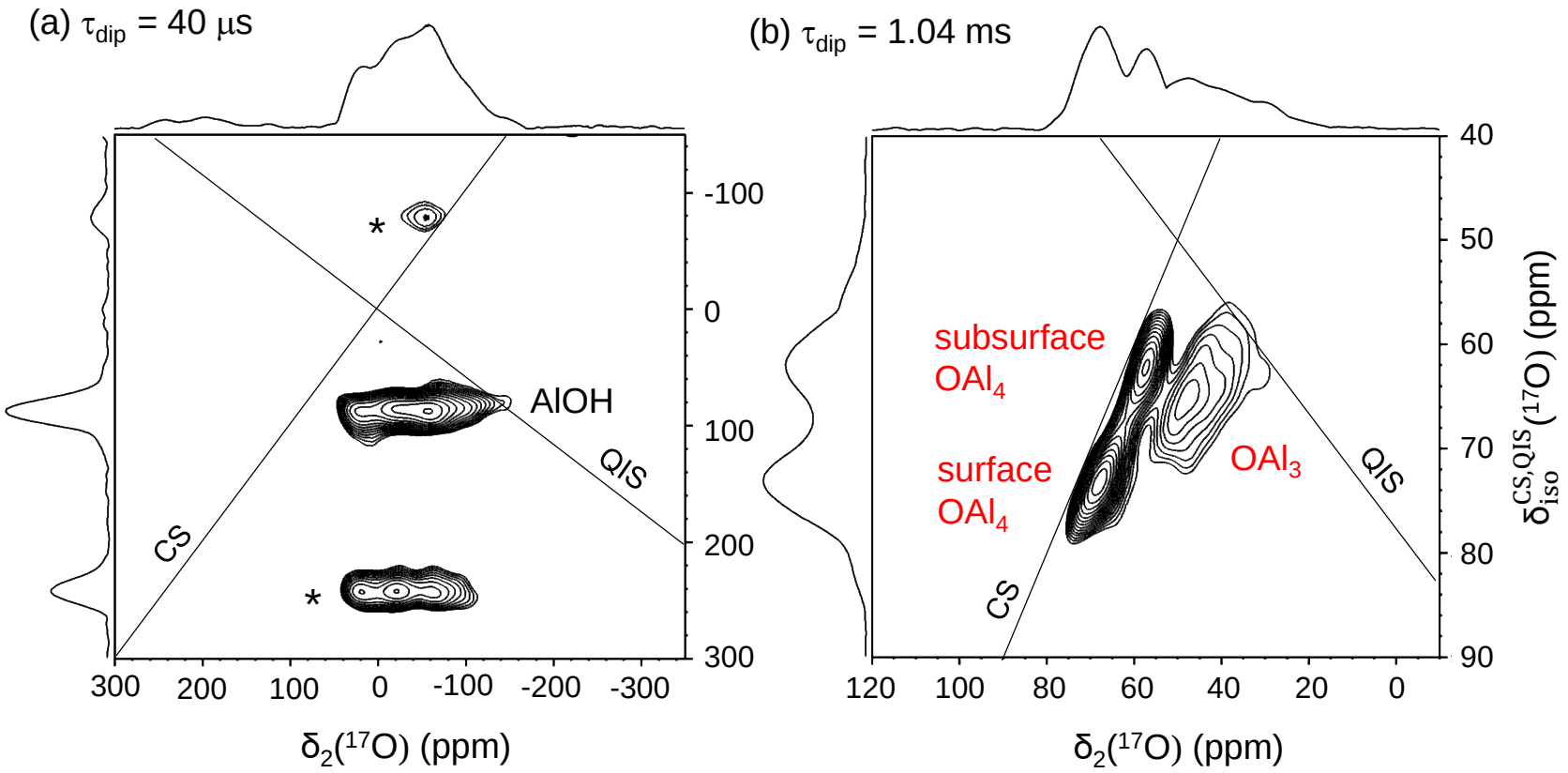

Fig.2. DNP-enhanced 2D $^{1}H \rightarrow {}^{17}O$ *D*-RINEPT-MQMAS-QCPMG spectra along with their skyline projections in both dimensions of γ-alumina enriched in ^{17}O isotope using grinding in zirconia jar for (a) 1 and (b) 15 min and then impregnated with 10 mM TEKPol solution. The spectra were acquired with τ_{dip} = (a) 40 μs and (b) 1.04 ms, and (a) 20 and (b) 15 QCPMG echoes. The symbol * denotes spinning sidebands. The CS axis and QIS direction are also displayed.

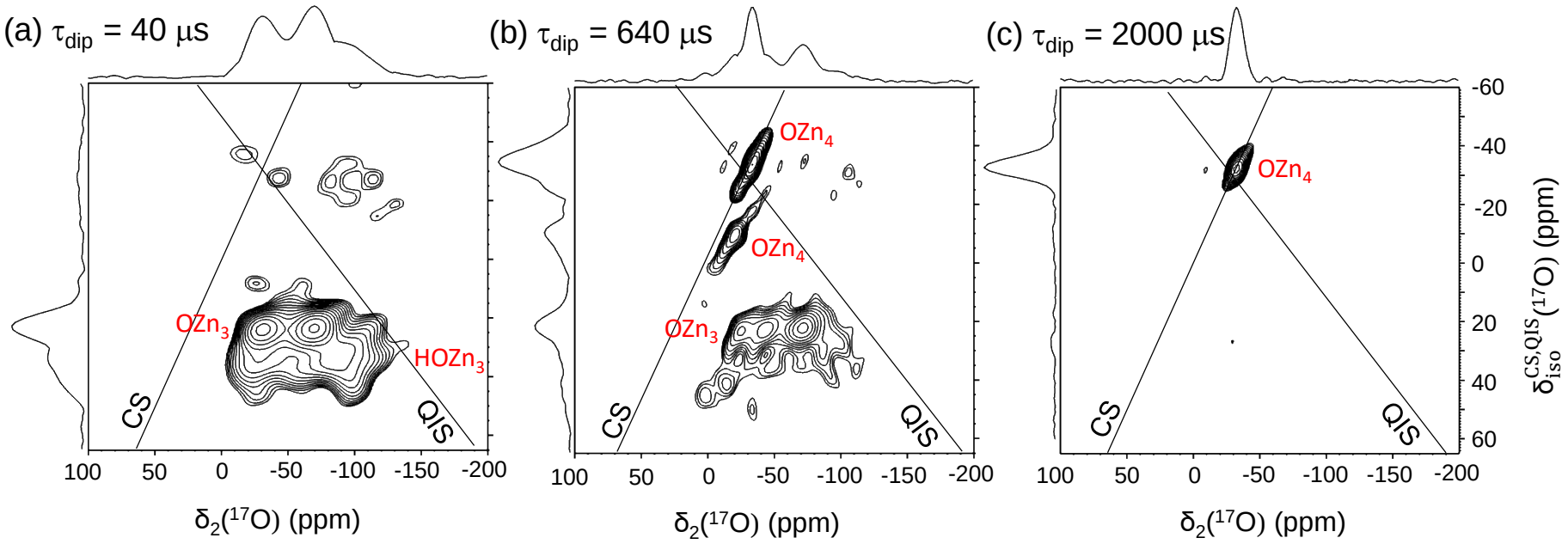

Fig.3. DNP-enhanced 2D $^{1}H \rightarrow {}^{17}O$ *D*-RINEPT-MQMAS-CPMG spectra along with their skyline projections in both dimensions of ZnO@DDA impregnated with 16 mM TEKPol solution. The spectra were acquired with τ_{dip} = (a) 40, (b) 640 and (c) 2000 μs, and (a) 20, (b) 19 and (c) 26 QCPMG echoes. The CS axis and QIS direction are displayed.

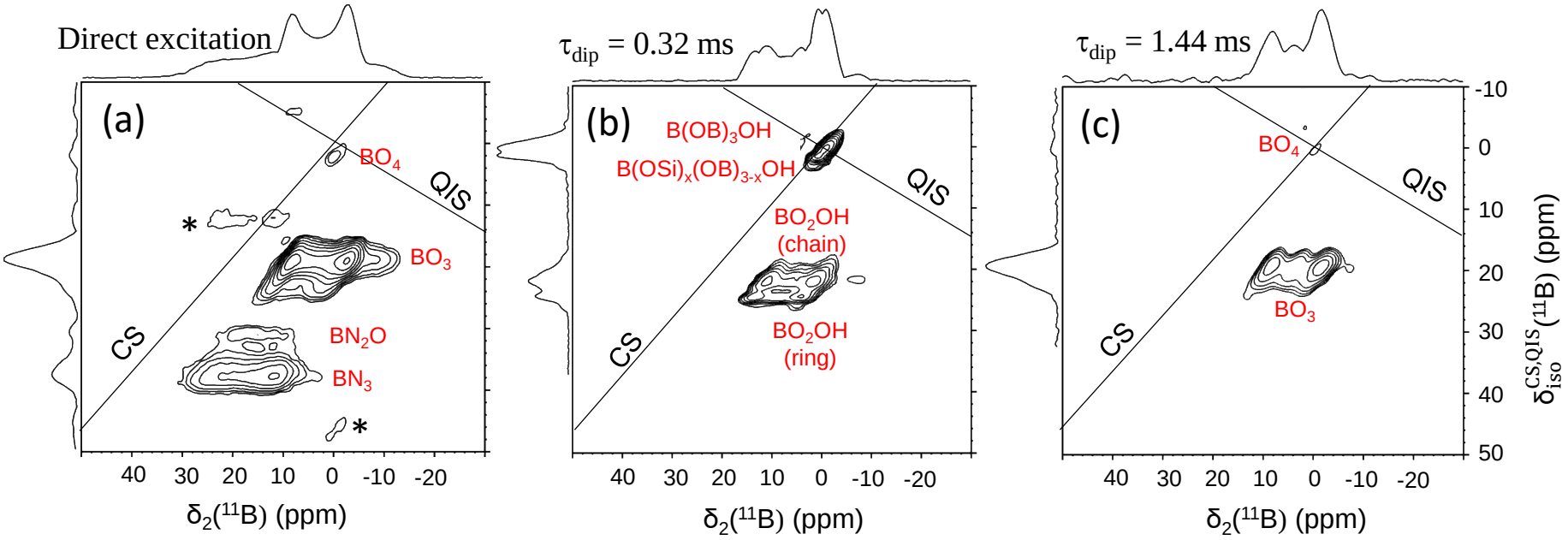

Fig.4. DNP-enhanced 2D ^{11}B MQMAS-CPMG spectra along with their skyline projections in both dimensions of BN-B_2O_3/SiO_2 impregnated with 10 mM TEKPol solution acquired using (a) the z-filter MQMAS technique and (b,c) the 2D ^{1}H→ ^{11}B *D*-RINEPT-MQMAS-QCPMG scheme with τ_{dip} = (b) 0.32 and (c) 1.44 ms, and 16 QCPMG echoes. The CS axis and QIS direction are displayed.